AIAA JOURNAL
Vol. 31, No. 5, May 1993

# Simulation of Three-Dimensional Liquid Sloshing Flows Using a Strongly Implicit Calculation Procedure

Kuo-Huey Chen*
*NASA Lewis Research Center, Cleveland, Ohio 44135*
and
Richard H. Pletcher†
*Iowa State University, Ames, Iowa 50011*

**A coupled strongly implicit solution strategy for unsteady three-dimensional free surface flows has been developed based on an artificial compressibility formulation for the incompressible Navier-Stokes equations. A pseudotime term has been used in the continuity equation to permit time-accurate calculations to be achieved. The scheme appears capable of tracking the free surface reasonably accurately inside a partially filled spherical container undergoing a general rotating motion characteristic of that experienced by a spin-stabilized satellite. Five different free surface calculations have been presented. Some of the results exhibit an interesting Reynolds number dependent oscillatory behavior that is believed to be physical, although no experimental results appear to be available for verification to date.**

## Introduction

THE liquid sloshing motion inside a container has long been of interest to engineers and researchers. Liquid sloshing occurs in many important practical applications such as in oil tankers, railroad tank cars, missiles, satellites, and spacecraft.[1-3] A particular goal of the present study has been the simulation of sloshing motion in a spherical container undergoing motion characteristic of that experienced aboard a spin-stabilized satellite. The major concern about the liquid sloshing motion within a container is that a substantial periodic force may be generated that may affect the stability of the moving vehicle. If the sloshing frequency is near the natural frequency of the vehicle structure, resonance may increase the likelihood of structural damage or instability resulting from the motion.

The sloshing motion of liquid usually involves the presence of a free surface that is the interface between the liquid and air or other type of gas. The presence of the free surface adds another difficulty in analysis to an already complicated fluid motion, since the free surface position usually is not known *a priori* and has to be determined as part of the solution. The container may undergo several different kinds of motion ranging from a simple linear acceleration or rotation to more complicated combinations of these. To conveniently analyze the motion, it is usually necessary to transform the governing equations to a noninertial coordinate system.[4] The motion of the liquid is generally three dimensional, time dependent, and sufficiently complex that no major simplification to the general equations (incompressible Navier-Stokes equations) is possible. The accurate simulation of such motion is a formidable problem primarily because of the computational resources required, and few, if any, three-dimensional time-dependent simulations have been reported in the literature.

Chakravarthy[5] investigated laminar incompressible flow within rotating liquid-filled shells under rotation but without the presence of free surfaces. Vaughn et al.[4] solved the three-dimensional incompressible Navier-Stokes equations for a fluid-filled cylindrical canister that was spinning and nutating. In their work, the equations were transformed to a noninertial frame. Again, the container was completely filled with liquid and no free surface was present. In a review of the literature, very few articles dealing with the liquid sloshing within a spherical container were found. Perhaps most relevant to the present study is the work of Kassinos and Prusa,[6] where a general motion of a spherical container was accounted for by a complete coordinate transformation using several successive axis rotations and a translation. Some liquid spin-up problems have been restricted to either the rectangular[7] or the cylindrical[8] configurations.

The present study uses a surface fitting approach[6,9,10] for the free surface and the artificial compressibility formulation of the equations. In this method a fictitious time-derivative of pressure is added to the continuity equation so that the solution of the set of conservation equations can be marched in time. Originally, this method was thought to be only applicable to steady flow problems.[11] For these, the entire time dependence was fictitious, but the solution approached the correct steady-state solution asymptotically with time. More recently, investigators[12-14] have suggested that the procedure can be made accurate with respect to time by considering the timelike variable appearing in the fictitious time term added to the continuity equation to be a pseudotime. For each physical time step, the pseudotime is advanced several increments in an iterative fashion. When the variables no longer change with pseudotime, the fictitious time term is zero and the equations satisfy the compatibility condition for incompressible flow at the specified physical time. The coordinate treatment of Kassinos and Prusa,[6] which is applicable to sloshing phenomena under a variety of conditions, is adopted in this study. A coupled strongly implicit procedure (CSIP), initially proposed by Stone[15] and Weinstein et al.,[16] is used to solve the resulting algebraic system of equations with the specified boundary conditions. A similar solution procedure has been used previously by the present authors to solve coupled two-dimensional equations and was found to be efficient and robust for several diverse problems.[17] Unsteady results for five liquid sloshing problems in a rotating half-filled spherical container are presented. In the following sections, the mathematical formula-

Presented as Paper 91-1661 at the AIAA 22nd Fluid Dynamics, Plasmadynamics, and Lasers Conference, Honolulu, HI, June 24-27, 1991; received Jan. 27, 1992; revision received Sept. 25, 1992; accepted for publication Sept. 26, 1992. 

*Senior Research Associate; currently, Senior Research Associate, Ohio Aerospace Institute, 22800 Cedar Point Road, Brook Park, OH 44142. Member AIAA.

†Professor, Department of Mechanical Engineering. Member AIAA.

tion, boundary conditions, numerical solution algorithm, and results will be discussed in detail.

## Mathematical Formulation

### Governing Equations

The incompressible Navier-Stokes equations with an isothermal condition can be written as

$$\frac{\partial u_i}{\partial x_i} = 0 \tag{1}$$

$$\frac{\partial u_i}{\partial t} + u_j\frac{\partial u_i}{\partial x_j} = -\frac{1}{\rho}\frac{\partial p}{\partial x_i} + \nu\frac{\partial^2 u_i}{\partial x_j \partial x_j} - g_i \tag{2}$$

where $u_i$ is the velocity component, $p$ is the thermodynamic pressure, $g_i$ is the acceleration of gravity, $\rho$ is the density (constant), $\nu$ is the kinematic viscosity, and $x_i$ represents the spatial coordinates.

At least two different approaches can be used to formulate this problem for numerical solution. First, Eqs. (1) and (2) can be solved in the form as indicated together with the proper treatment of the boundary conditions in accordance with the rotating-nutating motion of the container at any instant of time. Ideally, this treatment is workable for a simple motion of the container but will become impractical and difficult for describing the motion and interpreting the results if a general rotating-nutating motion is encountered. Actually, such a general motion can arise in the interaction between a satellite structure and the liquid sloshing in a partially filled container. Therefore, it is more appropriate to handle the general motion of the container with terms within the equations themselves. That is, the motion of the container relative to an inertial frame can be implicitly accounted for by proper coordinate transformations. This is the second approach and the one that will be adopted in this study. A schematic diagram of the partially filled rotating-nutating container is shown in Fig. 1.

Following the approach outlined in Kassinos and Prusa,[6] several steps are needed to transform the governing equations from an inertial to a noninertial frame. They are described in the following several sections. In addition to those transformations, a generalized nonorthogonal coordinate transformation is applied to the resulting equations to handle the irregular geometry of the boundaries.

*Rotating-Nutating Coordinates: $x_2$ Coordinate System*

The original three-dimensional incompressible equations will be labeled with a subscript 0 to indicate that they are in the $x_0$ inertial frame and rewritten as

$$\frac{\partial u_{0i}}{\partial x_{0i}} = 0 \tag{3}$$

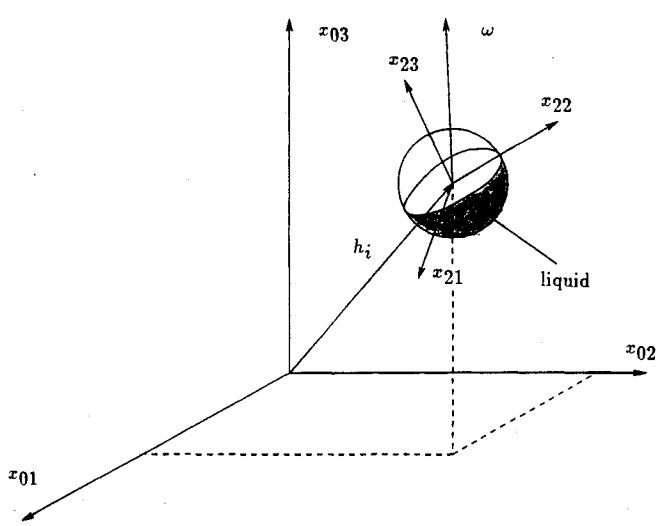


**Fig. 1 Schematic of a partially filled rotating-nutating container moving relative to an inertial frame.**

$$\frac{\partial u_{0i}}{\partial t_0} + u_{0j}\frac{\partial u_{0i}}{\partial x_{0j}} = -\frac{1}{\rho}\frac{\partial p}{\partial x_{0i}} + \nu\frac{\partial^2 u_{0i}}{\partial x_{0j}\partial x_{0j}} - g_{0i} \tag{4}$$

The container may undergo a motion with nonzero angular velocities or accelerations with respect to each axis at any instant of time. If a coordinate frame $x_1$ is attached to the spacecraft (or other vehicle) undergoing this general motion, then three successive coordinate rotations will reflect this motion. The procedure to perform the three coordinate rotations is described in detail in Chen[18] and Chen and Pletcher.[19] Also, since the container may be attached to another structure (satellite or spacecraft, for example) by an elastic bar, another translation is required to move the origin of the $x_1$ coordinate to the location of the container by the length of the elastic bar $h_i$. After combining the three successive rotations and the translation, the relationship between $x_0$ and $x_2$ is

$$x_{2i} = \alpha_{ji}x_{0j} - h_i \quad \text{or} \quad x_{0i} = \alpha_{ij}(x_{2j} + h_j) \tag{5}$$

where $\alpha_{ij}$ represents the elements of a $3 \times 3$ transformation matrix $[T]$, between the preceding $x_0$ and $x_1$ frames, resulting from the previous successive rotations. The transformation matrix $[T]$ is expressed as follows:

$$[T] = \begin{bmatrix} C_2C_3 & S_1S_2C_3 - C_1S_3 & C_1C_3S_2 + S_1S_3 \\ C_2S_3 & S_1S_2S_3 + C_1C_3 & C_1S_2S_3 - S_1C_3 \\ -S_2 & S_1C_2 & C_1C_2 \end{bmatrix}$$

where $C_i = \cos\psi_i$ and $S_i = \sin\psi_i$.

After applying the chain rule to the derivative terms in Eqs. (3) and (4) using Eq. (5), the governing equations in the $x_2$ frame can be expressed as

$$\frac{\partial u_{2i}}{\partial x_{2i}} = 0 \tag{6}$$

$$\frac{\partial u_{2l}}{\partial t_2} - \dot{\alpha}_{il}\alpha_{ij}u_{2j} + [\dot{\alpha}_{ji}\alpha_{jk}(x_{2k} + h_k) - \dot{h}_i + u_{2i}]\frac{\partial u_{2l}}{\partial x_{2i}}$$

$$= -\frac{1}{\rho}\frac{\partial p}{\partial x_{2l}} + \nu\frac{\partial^2 u_{2l}}{\partial x_{2j}\partial x_{2j}} - g_{2l} \tag{7}$$

where $u_{2i} = \alpha_{ji}u_{0j}$, $g_{2l} = \alpha_{il}g_{0i}$, $\dot{h}_i = \mathrm{d}h_i/\mathrm{d}t$, and $\dot{\alpha}_{il} = \mathrm{d}\alpha_{il}/\mathrm{d}t$.

To more conveniently describe the solutions and apply the boundary conditions, a new relative velocity is defined as follows:

$$u_{2l'} = u_{2l} + \dot{\alpha}_{ji}\alpha_{jk}(x_{2k} + h_k) - \dot{h}_i$$

This new relative velocity is always zero at the wall of the container no matter what kind of motion the container may undergo. The introduction of this new relative velocity can greatly simplify the treatment of the boundary conditions. Substituting the preceding definition of the relative velocity into Eqs. (6) and (7) and omitting the primes, we have the following equations written in terms of relative velocity components:

$$\frac{\partial u_{2i}}{\partial x_{2i}} = 0 \tag{8}$$

$$\frac{\partial u_{2l}}{\partial t_2} + u_{2i}\frac{\partial u_{2l}}{\partial x_{2i}} - 2\beta_{cr,li}u_{2i} - \beta_{t,li}(x_{2i} + h_i) - \beta_{cp,li}(x_{2i} + h_i)$$

$$= -\frac{1}{\rho}\frac{\partial p}{\partial x_{2l}} + \nu\frac{\partial^2 u_{2l}}{\partial x_{2j}\partial x_{2j}} - g_{2l} + E_l \tag{9}$$

where $\beta_{cr,li} = \dot{\alpha}_{jl}\alpha_{ji}$, $\beta_{t,li} = \ddot{\alpha}_{jl}\alpha_{ji}$, $\beta_{cp,li} = \dot{\alpha}_{kl}\dot{\alpha}_{ki} - \dot{\alpha}_{kl}\dot{\alpha}_{nj}\alpha_{kj}\alpha_{ni}$, $E_l = 2\dot{\alpha}_{il}\alpha_{ij}\dot{h}_j - \ddot{h}_l$, $\ddot{h}_l = \mathrm{d}^2h_l/\mathrm{d}t^2$, and $\ddot{\alpha}_{jl} = \mathrm{d}^2\alpha_{jl}/\mathrm{d}t^2$.

**Free Surface Tracking Coordinates: $x_3$ Coordinate System**

When the container undergoes a rotating-nutating motion, the free surface shape will change continuously with time. Equations (8) and (9) can be used to model this motion; however, a third coordinate rotation is preferred in this study for the following two reasons. First, the kinematic equation that is used in this study to update the free surface at each time step requires that the free surface height be a single-valued function of the other two coordinates. Therefore, it is important to keep this free surface a single-valued function by rotating the coordinates as required at each computational time step. Second, rotating the coordinates in response to changes in the orientation of the free surface facilitates the establishment of the computational grid by the present algebraic grid-generation scheme.

At any instant of time, the free surface may move to a new position with respect to the $x_2$ coordinates shown in Fig. 2. It is desirable to have the $x_{23}$ axis remain normal to the free surface in an average sense. One way to accomplish this is to let the $x_2$ coordinates rotate an angle $\phi_r$ counterclockwise about the $x_{22}$ axis and a successive counterclockwise rotation angle $\phi_r'$ about the $x_{31}'$ axis shown in Fig. 2. A transformation matrix $[S]$ is required to transform from the $x_2$ to the $x_3$ coordinates. The expression for this transformation matrix $[S]$ is

$$[S] = \begin{bmatrix} \cos\phi_r & \sin\phi_r \sin\phi_r' & -\sin\phi_r \cos\phi_r' \\ 0 & \cos\phi_r' & \sin\phi_r' \\ \sin\phi_r & -\cos\phi_r \sin\phi_r' & \cos\phi_r \cos\phi_r' \end{bmatrix}$$

The relationship between the $x_2$ and $x_3$ coordinates is

$$x_{2i} = s_{ij} x_{3j} \tag{10}$$

where $s_{ij}$ is an element of $[S]$.

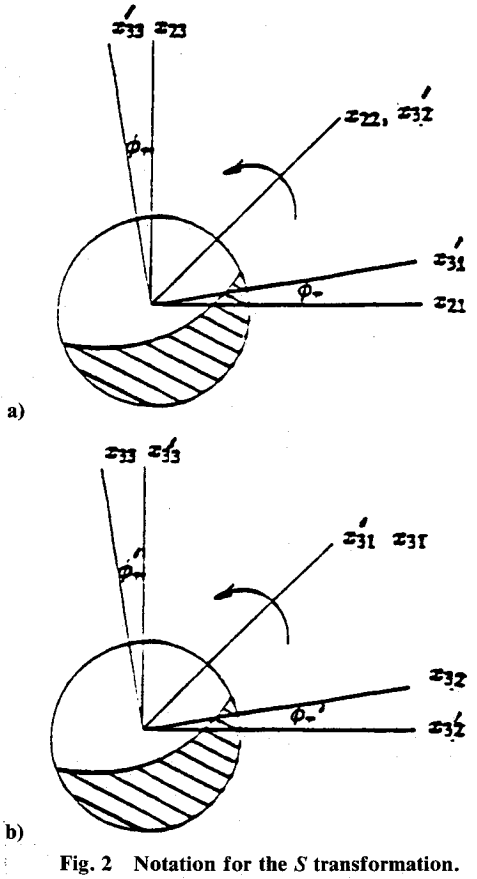


**Fig. 2 Notation for the $S$ transformation.**

The chain rule is then applied to Eqs. (8) and (9) using Eq. (10), and the resulting governing equations in the $x_3$ coordinates are

$$\frac{\partial u_{3i}}{\partial x_{3i}} = 0 \tag{11}$$

$$\frac{\partial u_{3n}}{\partial t_3} + (u_{3i} + f_{ij} x_{3j}) \frac{\partial u_{3n}}{\partial x_{3i}} - (f_{ni} + 2\lambda_{ni}) u_{3i} - \tau_{1,ni} x_{3i} - \tau_{2,ni} h_i = -\frac{1}{\rho} \frac{\partial p}{\partial x_{3n}} + \nu \frac{\partial^2 u_{3n}}{\partial x_{3j} \partial x_{3j}} - g_{3n} + E_n \tag{12}$$

where $u_{3j} = s_{ij} u_{2i}$, $g_{3n} = s_{ln} g_{2l}$, $f_{ij} = \dot{s}_{ki} s_{kj}$, $\lambda_{ni} = \beta_{cr,lj} s_{ji} s_{ln}$, $\tau_{1,ni} = (\beta_{t,lj} + \beta_{cp,lj}) s_{lm} s_{ji}$, $\tau_{2,ni} = (\beta_{t,li} + \beta_{cp,li}) s_{ln}$, and $E_n = s_{ln} E_l$.

**Generalized Nonorthogonal Coordinates: $z$ Coordinate System**

It is desirable to establish a new coordinate system having the property that the coordinate lines fit the boundaries of the problem domain of interest, i.e., the liquid itself enclosed by the container wall and the free surface. Let this new coordinate system be designated by $(\tau, z_i)$. The relationship between the $(t_3, x_{3i})$ and $(\tau, z_i)$ coordinate systems can be expressed as

$$\tau = t_3 \qquad z_i = z_i(x_{31}, x_{32}, x_{33}, t_3)$$

By applying the chain rule to the time and spatial derivative terms, the final governing equations in generalized nonorthogonal coordinates can be written as

$$\eta_{j,i} \frac{\partial u_{3i}}{\partial z_j} = 0 \tag{13}$$

$$\frac{\partial u_{3n}}{\partial \tau} + (\dot{z}_j + \eta_{j,i} u_{3i} + \eta_{j,k} f_{ik} x_{3k}) \frac{\partial u_{3n}}{\partial z_j} - (f_{ni} + 2\lambda_{ni}) u_{3i} + \eta_{j,n} \frac{\partial p}{\partial z_j} - \frac{1}{Re} \left( \eta_{j,i} \eta_{k,i} \frac{\partial^2 u_{3n}}{\partial z_j \partial z_k} + \eta_{k,ii} \frac{\partial u_{3n}}{\partial z_k} \right) = \tau_{1,ni} x_{3i} + \tau_{2,ni} h_i - g_{3n} + E_n \tag{14}$$

where $\eta_{i,j} = \partial z_i / \partial x_{3j}$ and $\eta_{i,jj} = \partial^2 z_i / \partial x_{3j} \partial x_{3j}$ are the metric terms, and $\dot{z}_i = \partial z_i / \partial t_3$ is the grid speed term. The detailed expressions for the metric terms and the grid speed terms are documented in Chen.[18] It should be noted that Eqs. (13) and (14) have been nondimensionalized before performing the generalized nonorthogonal coordinates transformation by the following nondimensional quantities:

$$x_{3i}^* = \frac{x_{3i}}{L_{\text{ref}}}, \quad u_{3i}^* = \frac{u_{3i}}{V_{\text{ref}}}, \quad t^* = \frac{t}{t_{\text{ref}}}, \quad p^* = \frac{p - p_0}{p_{\text{ref}}} \tag{15}$$

where $L_{\text{ref}}$ is the radius of the sphere, $V_{\text{ref}}$ is the reference velocity (which will be defined later), $p_{\text{ref}} = \rho V_{\text{ref}}^2$, $t_{\text{ref}} = L_{\text{ref}} / V_{\text{ref}}$, and $p_0$ = atmospheric pressure or saturated vapor pressure above the free surface. The superscript asterisk has been dropped for convenience in Eqs. (13) and (14), and the Reynolds number $Re$ in Eq. (14) is defined as

$$Re = \frac{V_{\text{ref}} L_{\text{ref}}}{\nu}$$

## Boundary Conditions

All boundary conditions are treated implicitly. In general, except for no-slip boundaries, the governing equations are written at boundary points. There are only two types of boundaries for this three-dimensional configuration (see Fig. 3). They are the solid wall of the container and the free surface. Four boundary equations are required at each boundary to close the system of equations.

At the wall of the spherical container, a no-slip condition is used for three velocities ($u_{3i} = 0$) and the normal momentum

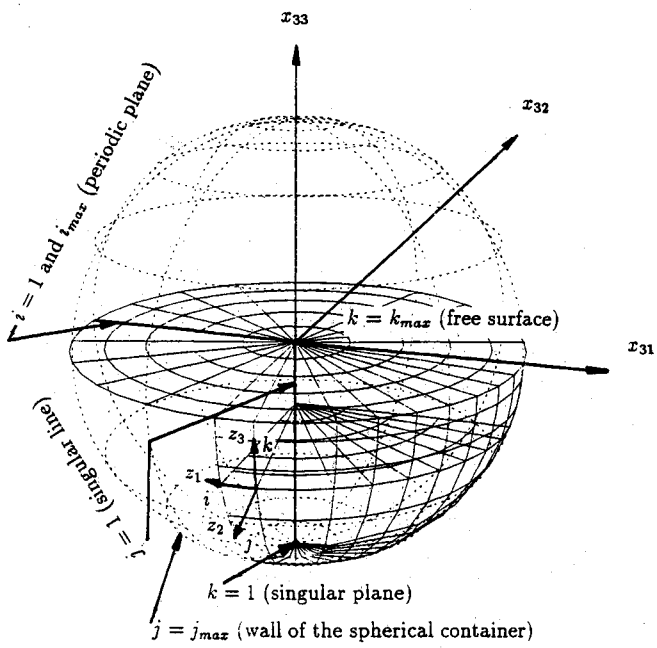


**Fig. 3 Coordinate system for liquid sloshing problem.**

equation for pressure. The normal momentum equation is formed by performing the inner product of the *local* unit normal vector and the three momentum equations, Eq. (14). The resulting normal momentum equation after simplifying with the no-slip condition can be found in Chen[18] and Chen and Pletcher.[19]

At the free surface boundary, strictly speaking, five equations are needed since one more equation is required for an additional unknown, i.e., the free surface position, which is part of the solution. The so-called dynamic equations will be discussed first. These equations, which will be coupled with the Navier-Stokes equations for the interior points, are derived based on the following conditions. First, it is assumed that the two tangential shear stresses along the free surface are zero since no external tangential forces are applied to the surface. Second, the normal shear stress must be continuous across the free surface boundary. Finally, the continuity equation must be satisfied at this boundary. For the continuous normal stress condition, a further assumption for air is made to only retain the pressure contribution to the normal stress equation, since the viscous stress contribution is small for air compared with the corresponding terms for the liquid.

These four equations in nondimensional form are the following:

1) Continuity equation:

$$\eta_{j,i}\frac{\partial u_{3i}}{\partial z_j} = 0 \tag{16}$$

2) Zero tangential shear stress (two equations):

$$\frac{\partial U_n}{\partial \tau_1} + \frac{\partial U_{\tau_1}}{\partial n} + U_{\tau_1}\kappa_1 = 0 \tag{17}$$

$$\frac{\partial U_n}{\partial \tau_2} + \frac{\partial U_{\tau_2}}{\partial n} + U_{\tau_2}\kappa_2 = 0 \tag{18}$$

3) Continuous normal shear stress:

$$p - \frac{2}{Re}\frac{\partial U_n}{\partial n} - \frac{1}{We}\kappa = 0 \tag{19}$$

where $n$, $\tau_1$, and $\tau_2$ denote distances normal to the free surface and along the first and second tangential directions at the free surface, respectively. The variables $U_n$, $U_{\tau_1}$, and $U_{\tau_2}$ denote velocity components along the $n$, $\tau_1$, and $\tau_2$ directions, respectively, at the free surface. The $\kappa_1$, $\kappa_2$, and $\kappa$ denote *local* curvature terms, and *We* is the Weber number defined as

$$We = \frac{\rho V_{\text{ref}}^2 L_{\text{ref}}}{\Gamma}$$

where $\Gamma$ is the surface tension coefficient. The detailed derivation of the preceding quantities can be found in Chen.[18]

Finally, the additional unknown, i.e., free surface position, is determined from the kinematic equation that is derived from the Lagrangian point of view.[20] Basically, it represents the fact that fluid particles that lie on the surface must remain on it. Letting $F$ be the free surface height that is a function of time and the $x_{31}$ and $x_{32}$ coordinates, the condition that a particle on the free surface must remain on the free surface can be written as

$$\frac{\mathrm{D}}{\mathrm{D}t_2}[F(x_{31}, x_{32}, t_3) - x_{33}] = 0$$

Using the chain rule to express this in terms of the generalized nonorthogonal coordinates gives the following representation for the free surface kinematic condition:

$$\begin{aligned}\frac{\partial F}{\partial \tau} &= (u_{33} + f_{3k}x_{3k}) \\ &\quad - [\dot{z}_1 + (u_{31} + f_{1k}x_{3k})\eta_{1,1} + (u_{32} + f_{2k}x_{3k})\eta_{1,2}]\frac{\partial F}{\partial z_1} \\ &\quad - [\dot{z}_2 + (u_{31} + f_{1k}x_{3k})\eta_{2,1} + (u_{32} + f_{2k}x_{3k})\eta_{2,2}]\frac{\partial F}{\partial z_2}\end{aligned} \tag{20}$$

In Eq. (20), the free surface coincides with the $z_3 = \text{const}$ surface (see Fig. 3).

The free surface kinematic equation, Eq. (20), was used to explicitly establish a new free surface position after the flow solution for the entire domain was obtained. Central differences were used to represent the spatial derivative terms in Eq. (20). Equation (20) is only valid for the interior points. At the edge of the free surface, i.e., $i = 1$, $i_{\max}$, $j = j_{\max}$, and $k = k_{\max}$, the second-order Lagrangian extrapolation formula was used in the physical domain in the $z_2$ (radial) direction to obtain the free surface positions for all $\theta$ directions from the free surface position at the interior points.

The implementation of the boundary "equations" discussed in this section is not trivial and can be seen in detail in Chen.[18] Also, there were several types of singularities in this coordinate system (see Fig. 3) where special treatment was necessary.[18,19]

## Numerical Solution Algorithm

### Artificial Compressibility Method

The final governing equations, Eqs. (13) and (14), together with the boundary equations at the wall and at the free surface, Eqs. (16–19), close the system of equations once the free surface position is updated by the kinematic equation, Eq. (20). In this study, a form of the artificial compressibility method (first proposed by Chorin[11]) was used to solve these equations. The four unknowns $u_{3i}$ and $p$ are obtained simultaneously by this procedure.

The first step is to add an artificial time derivative of pressure $\partial p/\partial \tau^*$ to the continuity equation. This artificial pressure term not only provides a linkage between the time variation of pressure and the divergence of the velocity but also insures that the coupled system is nonsingular if central differences are used in the continuity equation. The final equations become

$$\frac{\partial p}{\partial \tau^*} + \eta_{j,i}\frac{\partial u_{3i}}{\partial z_j} = 0 \tag{21}$$

and

$$\frac{\partial u_{3n}}{\partial \tau} + (\dot{z}_j + \eta_{j,i}u_{3i} + \eta_{j,i}f_{ik}x_{3k})\frac{\partial u_{3n}}{\partial z_j} - (f_{ni} + 2\lambda_{ni})u_{3i} + \eta_{j,n}\frac{\partial p}{\partial z_j} - \frac{1}{Re}\left(\eta_{j,i}\eta_{k,i}\frac{\partial^2 u_{3n}}{\partial z_j \partial z_k} + \eta_{k,ii}\frac{\partial u_{3n}}{\partial z_k}\right) = \tau_{1,ni}x_{3i} + \tau_{2,ni}h_i - g_{3n} + E_n \quad (22)$$

where $\tau^*$ is a pseudotime. Note that this pseudotime is also added to the free surface continuity equation, Eq. (16).

It is important to add this artificial time term to the continuity equation after the generalized coordinate transformation is applied instead of before if the grid is moving in time. Pan and Chakravarthy[14] have pointed out that for a moving grid system the divergence of the velocity would not be zero if this term was added before the generalized coordinate transformation even in steady-state calculations.

### Discretization of the Equations

The discretization will be described for the form of the equations given by Eq. (22). A first-order forward difference was used for the time terms. Central differences were used for the spatial derivative terms in the equations. All metric terms of the transformation were evaluated by second-order central differences satisfying the geometric conservation law.[21] The grid speed terms were evaluated by a first-order forward difference. All nonlinear terms were linearized by a Newton method.[22] The representation for the nonlinear convective term is illustrated as

$$\left(u_{3i}\frac{\partial u_{3n}}{\partial z_j}\right)^{n+1} \simeq (\bar{u}_{3i})^{n+1}\left(\frac{\partial u_{3n}}{\partial z_j}\right)^{n+1} + \left(\overline{\frac{\partial u_{3n}}{\partial z_j}}\right)^{n+1}(u_{3i})^{n+1} - \left(\bar{u}_{3i}\overline{\frac{\partial u_{3n}}{\partial z_j}}\right)^{n+1} \quad (23)$$

where $(\bar{u}_{3i})^{n+1}$ and $(\overline{\partial u_{3n}/\partial z_j})^{n+1}$ are the values from the previous iteration level of the current time level $n+1$. The linearization error was effectively removed by doing subiterations at each time level. After linearization, the four variables $u_{3i}$ and $p$ appear in all of the equations, and the resulting system of equations takes the following form:

$$A^b_{i,j,k}q_{i,j,k-1} + A^s_{i,j,k}q_{i,j-1,k} + A^w_{i,j,k}q_{i-1,j,k} + A^p_{i,j,k}q_{i,j,k} + A^e_{i,j,k}q_{i+1,j,k} + A^n_{i,j,k}q_{i,j+1,k} + A^t_{i,j,k}q_{i,j,k+1} = b_{i,j,k} \quad (24)$$

which can be rewritten in vector form as

$$[A]q = b \quad (25)$$

where the coefficients $A^b$ to $A^t$ are $4 \times 4$ matrices, and $q$ is the vector of unknowns (dependent variables), $(u_{3i}, p)^T$, and $b$ is the right-hand side vector. The difference molecule can be seen in Fig. 4. The $A$ are the coefficient matrices for the unknowns at the positions indicated in the figures. The resulting algebraic system of equations (25) coupled with the boundary equations was solved by the CSIP method, which will be described next.

### Coupled Strongly Implicit Procedure

Following Stone,[15] a general iterative formula for Eq. (25) may be obtained by adding an auxiliary matrix $[P]$ to each side of Eq. (25) and adding iteration numbers to $q$ as

$$[A + P]q^{n+1,k+1} = [P]q^{n+1,k} + b \quad (26)$$

where $n$ is the time level and $k$ the iteration level. In the SIP method of Stone[15] and Weinstein et al.,[16] $[P]$ is chosen that $[A + P]$ can be decomposed as

$$[A + P] = [L][U] \quad (27)$$

where $[L]$ and $[U]$ are, respectively, lower and upper triangular matrices, each of which has only four nonzero elements for the three-dimensional seven-point formula in each row. A partial cancellation parameter was introduced to reduce the influence of this extra $[P]$ matrix by a Taylor series expansion (see details in Stone[15] and Weinstein et al.[16]). After $[L]$ and $[U]$ are obtained, the following procedure is used to obtain the unknown vector $q$.

Letting $\delta^{n+1,k+1} = q^{n+1,k+1} - q^{n+1,k}$ and a residual vector $R^{n+1,k} = b - [A]q^{n+1,k}$, Eq. (26) can be written as

$$[L][U]\delta^{n+1,k+1} = R^{n+1,k} \quad (28)$$

Defining a provisional vector $W$ by $W^{n+1,k+1} = [U]\delta^{n+1,k+1}$, the solution procedure can be written in two steps:

Step 1:

$$[L]W^{n+1,k+1} = R^{n+1,k} \quad (29)$$

Step 2:

$$[U]\delta^{n+1,k+1} = W^{n+1,k+1} \quad (30)$$

The process represented by Eqs. (29) and (30) consists of a forward substitution to determine $W^{n+1,k+1}$ followed by a backward substitution to obtain $\delta^{n+1,k+1}$. The coefficient matrix $[A]$ and also the $[L]$ and $[U]$ matrices need to be updated at each iteration since they contain unknowns due to the linearization procedure.

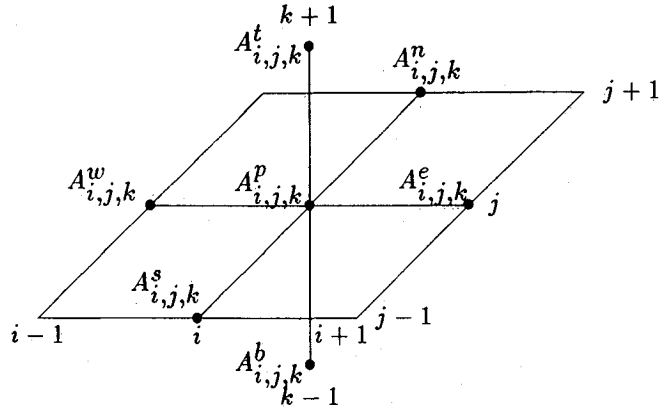


**Fig. 4 Three-dimensional computational molecule for $A^e_{i,j,k}$, $A^w_{i,j,k}$, ..., $A^p_{i,j,k}$.**

In the artificial compressibility method, the time term in the continuity equation is artificial (in pseudotime) even for time accurate calculations. It was found that convergence was enhanced by using a *local* pseudotime. This local pseudotime was determined based on the following criterion:

$$(\Delta\tau^*)_{i,j,k} \simeq \frac{\sigma}{\Sigma|\lambda_{i,j,k}|} \tag{31}$$

where $\lambda_{i,j,k}$ are the off-diagonal coefficient terms in the continuity equation, and the summation is over the six neighboring points at each $i$, $j$, and $k$ location. The $\Delta\tau^*$ is a local value and varies in space. The $\sigma$ is a constant to further control the time step. The choice of $\sigma$ is problem dependent. Usually a value of the order of one will give satisfactory results.

The convergence at each physical time step was based on the maximum value of the divergence of the velocity field. For the results presented here, this criterion is

$$|\nabla \cdot V| = \left|\eta_{j,i}\frac{\partial u_{3i}}{\partial z_j}\right| \leq 5 \times 10^{-4} \tag{32}$$

The solution procedure for the three-dimensional liquid sloshing flow calculations can be summarized as follows:

1) Set initial conditions.

2) Update the free surface position at each time step by the kinematic equation based on the flow solution at the previous time step.

3) Generate the grid under the new free surface position.

4) Construct the coefficient matrix $[A]$ and the right-hand side vector $\boldsymbol{b}$.

5) Call the CSIP solver to update solution ($u_{3i}$, $p$); go back to step 4 and subiterate (until convergence) to create a divergence-free field at each time step.

6) Go back to step 2 and move to the next time step.

## Results and Discussion

Before solving the more complicated three-dimensional unsteady liquid sloshing problems, the present algorithm was evaluated by solving the three-dimensional driven cavity problem for a Reynolds number of $1 \times 10^2$. The steady-state results were compared against the data in the literature and satisfactory agreement was observed.[18] Several cases for which the steady-state solution is known analytically will be discussed in the following sections.

### Axisymmetric Spin Up

Three axisymmetric spin up problems were studied. For this type of spin up, the tank rotates with respect to its own axis of symmetry ($h_i = 0$). Because of the symmetry of this problem, the solution should be independent of position in the circumferential direction. This provides one easy check on the validity of the code. As the spinning is initiated, the liquid and free surface begin to move relative to the container and eventually reach a steady-state equilibrium condition in which solid-body rotation prevails. Computations were made for three different types of spin up, all for normal Earth gravitational acceleration. The three types of spin up are described as follows:

1) Initially capped spin up: Initially, the spherical container half-filled with a liquid has been spun about a specified rotation axis in a constant rotational speed and has reached a solid-body rotation. A cap covers the liquid surface to prevent it from rising up. At time zero, the cap is suddenly removed (or broken) and the liquid surface starts to rise (or drop) until another equilibrium position is reached. The initial absolute velocity is distributed according to the condition of the solid-body rotation. This case was computed for two values of Reynolds number.

2) Gradual spin up: At time zero, the spherical container half-filled with a liquid gradually starts to rotate with the rotational speed from zero to a desired constant value about a specified rotation axis. The initial absolute velocity is zero everywhere.

3) Impulsive spin up: At time zero, the spherical container half-filled with a liquid impulsively starts to rotate with a constant rotational speed about a specified rotation axis (the axis of symmetry of the container, for the axisymmetric spin up case). The initial absolute velocity is zero everywhere except at the wall of the container.

For the same rotational speed of 60 rpm, the spin up phenomena were found to be quite different for these three spin up types. Results for these three axisymmetric spin up cases are given next.

### Initially Capped Spin Up

This case was computed for two Reynolds numbers, $Re = 2.19 \times 10^1$ and $2.2547 \times 10^3$, where the Reynolds number is based on the radius of the sphere and a reference velocity equal to the radius times the rotational speed in radians per second. These two Reynolds numbers can be achieved through the rotation of a sphere 6.4 cm in radius at 60 rpm using glycerin and kerosene as the fluids, so the two cases will be referred to as the glycerin and kerosene cases. Other characteristic dimensionless parameters of the problem include the Froude and Weber numbers. The Weber number has been defined previously. The Froude number is $Fr = V_{\text{ref}}/\sqrt{gh}$, where $V_{\text{ref}}$ is the same as used in the Reynolds number, $h$ is the initial maximum free surface depth, and $g$ is the acceleration of gravity. The Froude number was 0.51 for both of these initially capped cases. For the $2.19 \times 10^1$ case, $We = 207.6$, and for $Re = 2.2547 \times 10^3$, $We = 284.9$. The capped spherical container was initially spun about its axis of symmetry at a constant rotational speed until solid-body rotation prevailed in the liquid. Since the liquid surface was covered by a cap, there was no free surface motion at all. The initial absolute velocity distribution is as follows:

$$V_r = 0 \qquad V_\theta = r\omega \qquad V_z = 0$$

where $V_r$ is the velocity component in the radial direction, $V_\theta$ is the velocity component in the circumferential direction, $V_z$ is the velocity component in the direction normal to the previ-

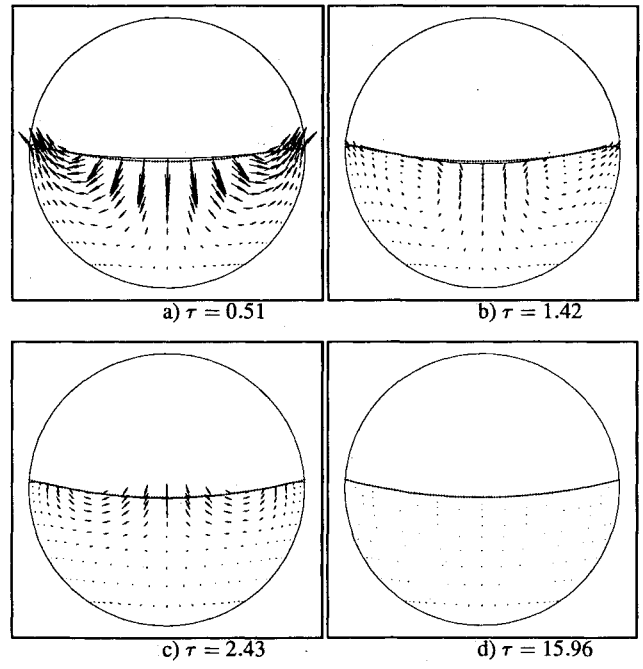


**Fig. 5 Selected velocity vector plots at $x_{22} = 0$ plane for the axisymmetric initially capped spin up of a spherical container half-filled with glycerin (dotted line indicates the steady-state analytical free surface position).**

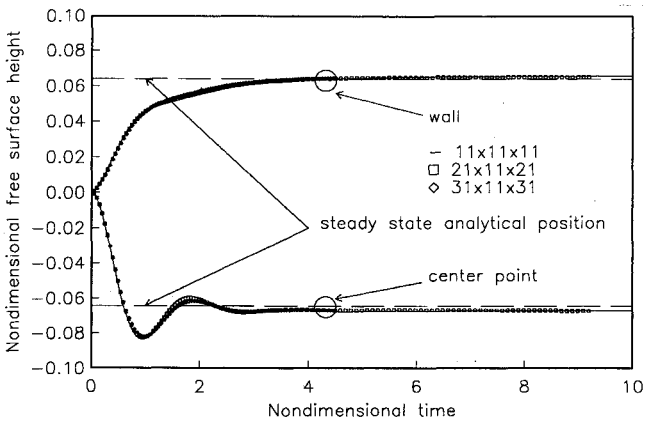


**Fig. 6 Time history of the nondimensional free surface height for the axisymmetric initially capped spin up of a spherical container half-filled with glycerin ($Re = 2.19 \times 10^1$).**

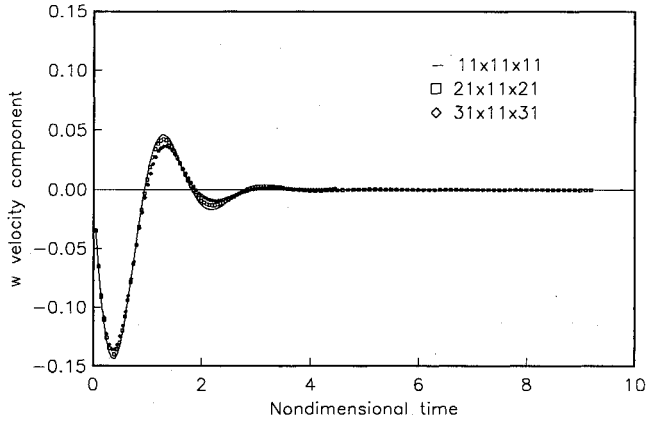


**Fig. 7 Time history of the $u_{23}$ velocity component on the free surface at the center of rotation for the axisymmetric initially capped spin up of a spherical container half-filled with glycerin ($Re = 2.19 \times 10^1$).**

ous two directions, $r$ is the distance in the radial direction away from the line of symmetry, and $\omega$ is the rotational speed (60 rpm) (with regard to the $x_{23}$ axis). It should be noted that the governing equations were expressed in terms of the relative velocity (relative to the final solid-body rotation), and therefore $u_{3i} = 0$ was actually used as the initial condition for velocities.

At time zero, the cap is suddenly removed (or broken) and the free surface starts to rise, from its initial position near the wall of the container and drop near the center of the free surface in response to the sudden change of the pressure field. Some selected velocity vector plots illustrating the general flow pattern at different times are shown in Fig. 5. The results shown are in the $x_{22} = 0$ plane. The time shown in the figures has been nondimensionalized using a characteristic time based on the radius of the container and the rotational speed at the wall. The dotted lines inserted in Fig. 5 indicate the analytical steady-state equilibrium (relative to the $x_2$ frame) free surface position. The analytical steady-state equilibrium free surface solutions were derived by the present authors and are listed in Chen.[18] The velocities are largest near the free surface and significantly smaller near the bottom of the container. As time continues, the fluid eventually passes (or overshoots) the equilibrium position. By time $\tau = 1.62$, the magnitude of the flow has been reduced, and the flow pattern has begun to reverse itself. This can be seen in Fig. 5b and more clearly in Fig. 5c. This flow continues to oscillate about the equilibrium position but damps very quickly until the new equilibrium position is reached at about $\tau = 15.96$ in Fig. 5d (see also Fig. 6). It should be noted that the magnitude of the velocities in Fig. 5d has become very small as the final solid-body rotation is approached. The velocities shown here are relative to the solid-body rotation expected at steady state, as pointed out in a preceding section. The steady-state numerical free surface position matches exceptionally well with the analytical solution.

To permit a more detailed analysis of the flow pattern under this spin-up condition, the time histories of the free surface positions at the wall of the container and at the center of the free surface and the $x_{23}$ component of the velocity were recorded for three different grids, i.e., $11 \times 11 \times 11$, $21 \times 11 \times 21$, and $31 \times 11 \times 31$. Figure 6 shows the free surface position at the wall and at the center of the free surface for glycerin during the spin-up process. The free surface position can be seen to oscillate about the equilibrium position. This oscillation is damped out quickly by the viscosity of the fluid. Figure 7 illustrates the same phenomena but shows the time evolution of the component of the velocity normal ($x_{23}$ component) to the free surface at the center of the container. The grid refinement study indicated in Figs. 6 and 7 shows that the unsteady free surface positions and velocity were relatively insensitive to the grid distribution in the circumferential and height (vertical) directions. It is well known that, for viscous free surface flow simulations, there exists an extremely thin boundary layer (or singularity) near the liquid-gas-solid contact line. In our grid refinement study, the effect of this singularity tended to become more evident and eventually caused the numerical calculations to break down as the grid spacing in the radial direction was refined.

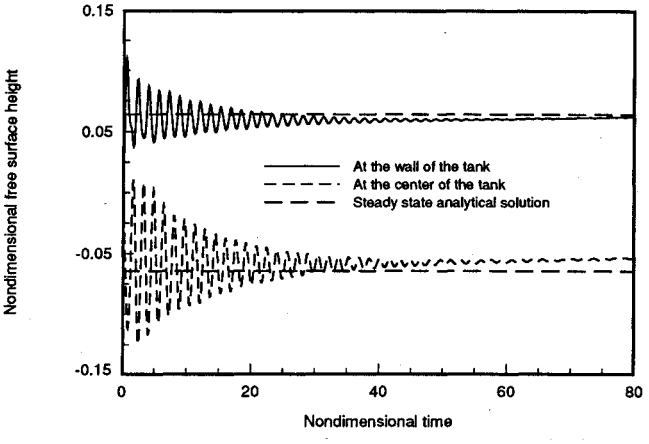


**Fig. 8 Time history of the nondimensional free surface height for the axisymmetric initially capped spin up of a spherical container half-filled with kerosene ($Re = 2.2547 \times 10^3$).**

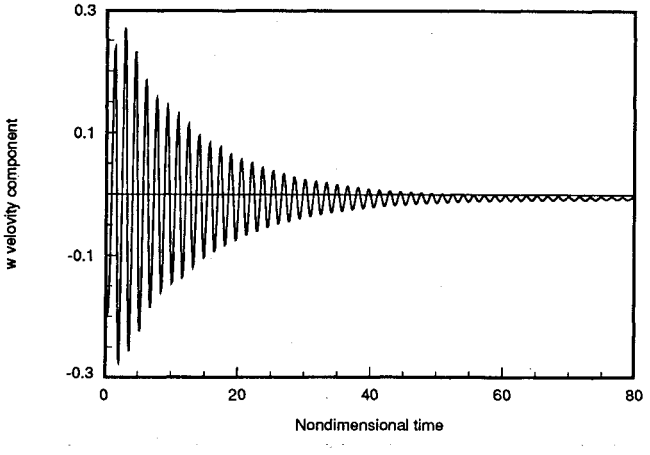


**Fig. 9 Time history of the $u_{23}$ velocity component on the free surface at the center of rotation for the axisymmetric initially caped spin up of a spherical container half-filled with kerosene ($Re = 2.2547 \times 10^3$).**

For this spin-up problem, the number of subiterations at the first time step were about 50 but then quickly dropped to less than 10 after 20 time steps and finally became 1 as the solution approached the final steady state. It took about 2 h of CPU time on the Apollo DN 10,000 workstation for the coarse grid case. A nondimensional time step of 0.015 was used throughout the calculation.

The initially capped spin-up calculations were repeated for a Reynolds number of $2.2547 \times 10^3$. This was achieved by keeping all rotation parameters the same and decreasing the kinematic viscosity of the fluid by a factor of about 100 to a value corresponding to the viscosity of kerosene. The final analytical equilibrium free surface position is then expected to be the same as for the glycerin case. With this less viscous fluid, the flow pattern was found quite similar to the preceding case and will not be repeated here; however, several interesting results deserve further discussion.

Figure 8 indicates the variation of the free surface position at the wall and tank center as a function of nondimensional time during the spin-up process for kerosene. Since the viscosity of kerosene is a factor of 100 less than that of glycerin, the free surface oscillations appear to damp out much more slowly than was observed for glycerin. This behavior is believed to be real, although no experimental data have been found to date to clarify this point. The final computed steady-state position of the free surface agrees reasonably well with the analytical solution. Figure 9 shows the computed velocity component normal to the free surface at the center of the container as a function of time. Slowly damped oscillatory motion is evident. The spin up with kerosene took about four times longer than

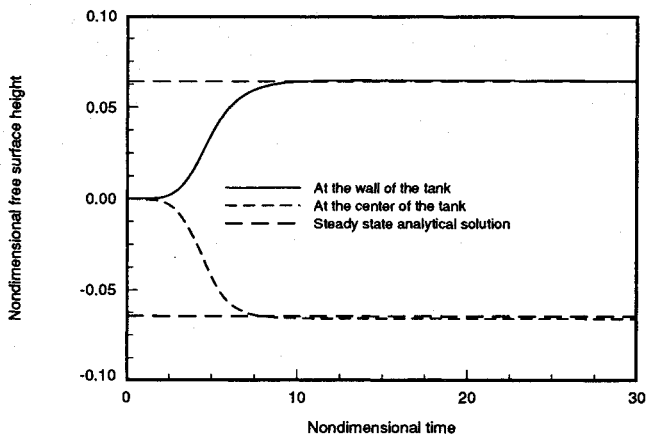


**Fig. 10 Time history of the nondimensional free surface height for the axisymmetric gradual spin up of a spherical container half-filled with glycerin ($Re = 2.19 \times 10^1$).**

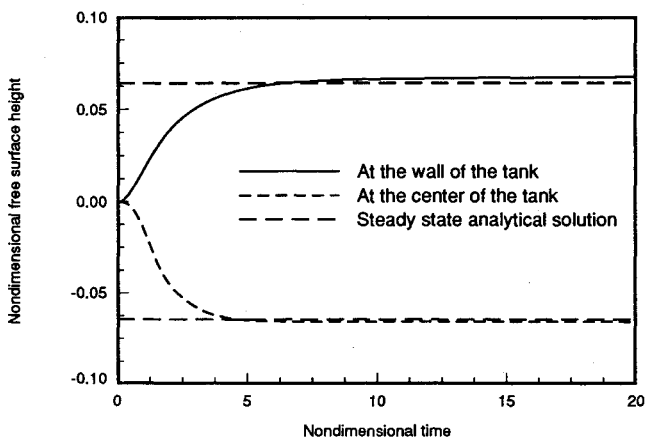


**Fig. 11 Time history of the nondimensional free surface height for the axisymmetric impulsive spin up of a spherical container half-filled with glycerin ($Re = 2.19 \times 10^1$).**

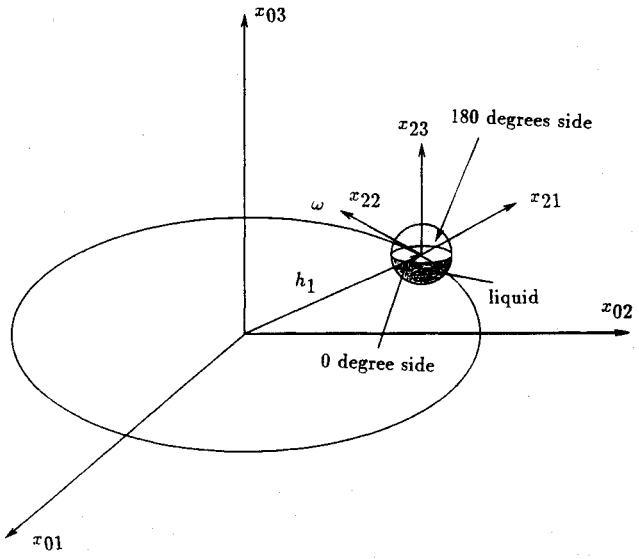


**Fig. 12 Schematic for asymmetric spin up; container half-filled with glycerin.**

that with glycerin to reach final steady-state solid-body rotation (both cases had the same reference time, and this was estimated from the plots shown previously).

The kerosene calculations were made with the same grid as used to obtain the glycerin results. During the course of early computations, it was found that the free surface developed a sawtoothed profile of small amplitude in the radial direction that appeared to slow convergence at each time step. The sawtoothed profile might have been due to the use of central differences in the spatial derivative terms in the kinematic equation at the higher Reynolds number. If the use of central differences at high Reynolds numbers was the source of the problem, it could have been remedied by the use of a finer grid that, of course, would have increased the required computational effort considerably. Instead, a small amount of smoothing was added to remove this undesired profile and stabilize the calculation. The smoothing was of the following form:

$$F^{\text{new}} = F^{\text{old}} + s\left(\frac{\partial^2 F^{\text{old}}}{\partial z_2^2}\right) \tag{33}$$

where $s$ is the smoothing parameter, $F$ is the free surface height function (see the free surface kinematic equation), and $z_2$ is the radial direction. A value of $s = 9 \times 10^{-3}$ was used for this case. The second derivative in Eq. (23) was represented, of course, in difference form. It should be noted that the use of the smoothing of the free surface height function $F$ for this calculation resulted in less than 1% loss of the initial total volume. Although this discrepancy may be considered insignificant for most purposes, ways of avoiding this loss deserve further study in the future.

### Gradual Spin Up; Liquid: Glycerin

As mentioned before, the high-frequency free surface oscillations were possibly due to natural overshoots arising from the sudden removal of the cap during the spin-up process. To further understand this phenomena, a third test for this configuration was conducted for glycerin again in the following way. The container was spun up with the rotational speed being gradually increased from 0 to 60 rpm by a sine function of time during the nondimensional time interval from zero to five. This rotational speed was specified as follows: $\omega = 30(\sin\theta + 1)$ rpm for $0 \le \tau \le 5$ where $\theta = (\pi/5)\tau - \pi/2$ and $\omega = 60$ rpm for $\tau > 5$.

Figure 10 indicates the variation of the free surface position at the wall and tank center as a function of nondimensional time during the gradual spin-up process. The oscillatory phe-

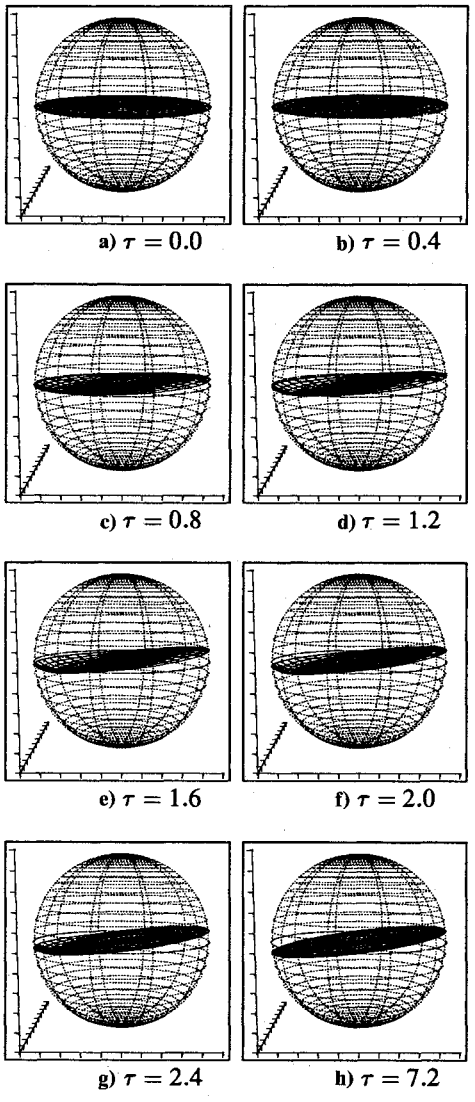


**Fig. 13 Selected free surface plots for the asymmetric initially capped spin up of a spherical container half-filled with glycerin.**

nomena in Fig. 6 disappeared and instead a nonoscillatory ramp-up of the free surface at the wall and a drop at the tank center were observed. The final steady-state free surface positions agree very well with the analytical solution.

#### Impulsive Spin Up; Liquid: Glycerin

At time zero, the spherical container half-filled with glycerin impulsively starts to rotate about its axis of symmetry. The initial absolute velocity was zero everywhere except at the wall of the container at which a rotational speed of 60 rpm was suddenly applied. Because of the use of the relative velocity in the formulation, a negative distribution of the solid-body rotation velocity was specified everywhere initially except at the wall where a zero relative velocity was specified. An $11 \times 11 \times 11$ grid was used again for this case. The free surface positions at the wall of the container and at the center of the free surface are shown in Fig. 11. No free surface overshoots were observed in this case. Being spun up impulsively, the flow reached the final steady-state equilibrium position earlier than for the preceding gradual spin-up case.

#### Asymmetric Spin Up

When the rotation arm $h_i$ is nonzero, the solutions will no longer be symmetric. A schematic diagram for this type of spin up is shown in Fig. 12. This case belongs to the initially capped spin-up type as explained in the preceding section. The same container as before was half-filled again with glycerin. It was initially covered by a cap and rotated in an orbit with a constant rotational speed under the condition of solid-body rotation. At time zero, the cap was removed to allow the liquid surface to move under this spinning condition. The rotational speed was 30 rpm, and the rotational arm $h_1$ ($x_{21}$ component of $h_i$) was 12.8 cm, which was twice that of the radius of the container. Based on the preceding physical quantities, the characteristic nondimensional parameters are

$$Re = 2.19 \times 10^1 \qquad Fr = 0.51 \qquad We = 207.6$$

where the reference velocity $V_{\text{ref}}$ was based on the rotational speed of the center of the container, i.e., $V_{\text{ref}} = \omega h_1$.

A $41 \times 11 \times 11$ grid was used to compute this case with the 41 points being placed in the circumferential direction. A constant nondimensional time step of 0.01 was used for this calculation. At the first time step, 170 subiterations were required for convergence, but the number of subiterations required dropped rapidly and varied between 10 and 15 for most of the calculation. Compared with the preceding axisymmetric cases, this calculation was more difficult in two respects. First, the free surface was asymmetric, and more grid points were required to resolve the solution in the circumferential direction. The solution would sometimes diverge suddenly if the resolution of the grid was not fine enough or if the grid distribution after the grid adaptation procedure contained a locally steep slope. Second, more computational effort was required to obtain the solution at each time step.

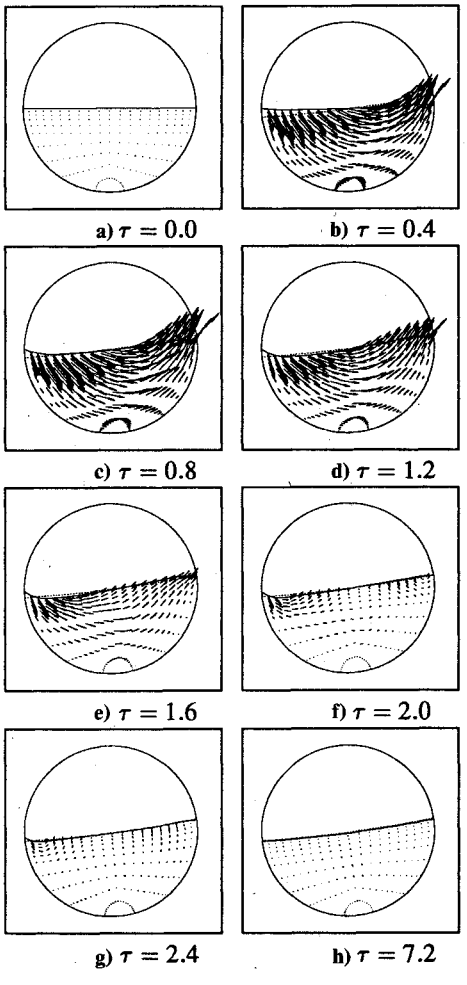


**Fig. 14 Selected velocity vector plots at $x_{22} = 0$ plane for the asymmetric initially capped spin up of a spherical container half-filled with glycerin (dotted line indicates the steady-state analytical free surface position).**

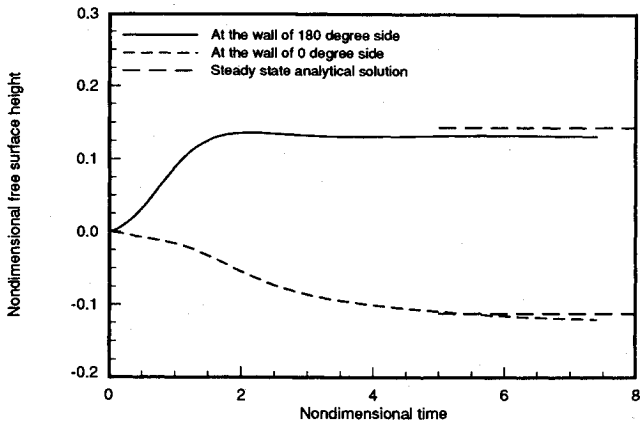


**Fig. 15 Time history of the nondimensional free surface height for the asymmetric initially capped spin up of a spherical container half-filled with glycerin.**

In this calculation, the value of $\phi_r$ in the free surface tracking coordinates was no longer zero. Therefore, the present test case also served as a check for this transformation. For this case, the computation was carried out until the final solid-body steady-state solutions were obtained.

In Fig. 13 a series of results showing the free surface position at different instants of time are presented. The centrifugal force is larger at the right-hand side (RHS) (far away from the spin axis) of the tank in Fig. 13 than at the left-hand side (LHS) (closer to the spin axis). In response to this sudden change, the free surface begins to rise at the RHS and to depress at the LHS from its initial position, becoming curved as can be seen in Figs. 13d–13f, and finally assumes a parabolic equilibrium shape at about $\tau = 7.2$.

Some selected velocity vector plots for different times in the $x_{22} = 0$ plane are shown in Fig. 14 with the analytical equilibrium free surface position[18] superimposed. The largest velocity vectors occurred near the free surface. The computation was carried out until the nondimensional time equaled 7.2, at which time solid-body rotation prevailed. The final free surface position can be seen to agree fairly well with the analytical solution.

Again, the numerical steady-state free surface positions at the wall of the container were plotted against the analytical solution. Figure 15 shows the time evolution of the free surface position at the wall for positions of 0 (LHS) and 180 (RHS) deg (see also Fig. 12). This plot indicates the free surface rise at the RHS and drop at the LHS from its initial position (equal to zero for a half-full container). The small discrepancy between the current numerical solution for the free surface position and the analytical solution is probably due to the relatively coarse grid used in this calculation. Further studies with a finer grid may help to resolve this discrepancy. This calculation took about 22 h of CPU time on the Apollo DN 10,000 workstation.

## Conclusions

A coupled strongly implicit solution strategy for unsteady three-dimensional free surface flows has been developed based on an artificial compressibility formulation for the Navier-Stokes equations. A pseudotime term has been used in the continuity equation to permit time accurate calculations to be achieved. The scheme appears capable of tracking the free surface reasonably accurately, although further verification of the procedure is desirable. An algebraic procedure for adjusting the grid between time steps has proven to be adequate. Five different free surface calculations have been reported. The initially capped cases exhibited an interesting Reynolds number dependent oscillatory behavior that is believed to be physical, although no experimental results appear to be available for verification to date.

## Acknowledgment

This research was supported by the Air Force Office of Scientific Research through Grant AFOSR-89-0403.

## References

[1]Peterson, L. D., Crawley, E. F., and Hansman, R. J., "Nonlinear Fluid Slosh Coupled to the Dynamics of a Spacecraft," *AIAA Journal,* Vol. 27, No. 9, 1989, pp. 1230–1240.

[2]Kana, D. D., "Validated Spherical Pendulum Model for Rotary Liquid Slosh," *Journal of Spacecraft and Rockets,* Vol. 26, No. 3, 1989, pp. 188–195.

[3]Van Schoor, M. C., Peterson, L. D., and Crawley, E. F., "The Coupled Nonlinear Dynamic Characteristics of Contained Fluids in Zero Gravity," AIAA Paper 90-0996-CP, April 1990.

[4]Vaughn, H. R., Oberkampf, W. L., and Wolfe, W. P., "Fluid Motion Inside a Spinning Nutating Cylinder," *Journal of Fluid Mechanics,* Vol. 150, Jan. 1985, pp. 121–138.

[5]Chakravarthy, S. R., "Numerical Simulation of Laminar, Incompressible Flow within Liquid Filled Shells," U.S. Army Research and Development Command, Ballistic Research Lab., Contract Rept. AR-BRL-CR-00491, Aberdeen Proving Ground, MD, Nov. 1982.

[6]Kassinos, A. C., and Prusa, J. M., "A Numerical Model for 3-D Viscous Sloshing in Moving Containers," *Proceedings of the ASME Winter Annual Meeting, Symposium on Recent Advances and Applications in Computational Fluid Dynamics,* edited by O. Baysal, Vol. 103, New York, 1990, pp. 75–86.

[7]Hirt, C. W., and Nichols, B. D., "Volume of Fluid (VOF) Method for the Dynamics of Free Boundaries," *Journal of Computational Physics,* Vol. 39, No. 1, 1981, pp. 201–225.

[8]Holler, H., and Ranov, T., "Unsteady Rotating Flow in a Cylinder with a Free Surface," Fluids Engineering Conference, Philadelphia, PA, May 6–8, 1968; also ASME Paper No. 68-FE-13, 1968.

[9]Miyata, H., "Finite-Difference Simulation of Breaking Waves," *Journal of Computational Physics,* Vol. 65, No. 1, 1986, pp. 179–214.

[10]Miyata, H., Sato, T., and Baba, N., "Difference Solution of a Viscous Flow with Free-Surface Wave About an Advancing Ship," *Journal of Computational Physics,* Vol. 72, No. 2, 1987, pp. 393–421.

[11]Chorin, A. J., "A Numerical Method for Solving Incompressible Viscous Flows Problems," *Journal of Computational Physics,* Vol. 2, No. 1, 1967, pp. 12–26.

[12]Rogers, S. E., and Kwak, D., "An Upwind Differencing Scheme for the Time-Accurate Incompressible Navier-Stokes Equations," AIAA Paper 88-2583, June 1988.

[13]Merkle, C. L., and Athavale, M., "Time-Accurate Unsteady Incompressible Flow Algorithm Based on Artificial Compressibility," AIAA Paper 87-1137, July 1987.

[14]Pan, D., and Chakravarthy, S., "Unified Formulation for Incompressible Flows," AIAA Paper 89-0122, Jan. 1989.

[15]Stone, H. L., "Iterative Solution of Implicit Approximations of Multi-Dimensional Partial Differential Equations," *SIAM Journal of Numerical Analysis,* Vol. 5, No. 3, 1968, pp. 530–558.

[16]Weinstein, H. G., Stone, H. L., and Kwan, T. V., "Iterative Procedure for Solution of Systems of Parabolic and Elliptic Equations in Three Dimensions," *I & EC Fundamentals,* Vol. 8, No. 2, 1969, pp. 281–287.

[17]Chen, K.-H., and Pletcher, R. H., "A Primitive Variable, Strongly Implicit Calculation Procedure for Viscous Flows at All Speeds," *AIAA Journal,* Vol. 29, No. 8, 1991, pp. 1241–1249.

[18]Chen, K.-H., "A Primitive Variable, Strongly Implicit Calculation Procedure for Two and Three-Dimensional Unsteady Viscous Flows: Applications to Compressible and Incompressible Flows Including Flows with Free Surfaces," Ph.D. Dissertation, Iowa State Univ., Ames, IA, 1990.

[19]Chen, K.-H., and Pletcher, R. H., "Simulation of Three-Dimensional Liquid Sloshing Flows Using a Strongly Implicit Calculation Procedure," AIAA Paper 91-1661, June 1991.

[20]Lamb, H., *Hydrodynamics,* Dover, New York, 1945.

[21]Hindmann, R. G., "Generalized Coordinate Forms of Governing Fluid Equations and Associated Geometrically Induced Errors," *AIAA Journal,* Vol. 20, No. 10, 1982, pp. 1359–1367.

[22]Anderson, D. A., Tannehill, J. C., and Pletcher, R. H., *Computational Fluid Mechanics and Heat Transfer,* McGraw-Hill, New York, 1984.